Interaction between a laminar starting immersed micro-jet and a parallel wall

Juan Martin Cabaleiro, Cecilia Laborde, and Guillermo Artana

Citation: Physics of Fluids (1994-present) **27**, 013601 (2015); doi: 10.1063/1.4905037
View online: http://dx.doi.org/10.1063/1.4905037
View Table of Contents: http://scitation.aip.org/content/aip/journal/pof2/27/1?ver=pdfcov
Published by the AIP Publishing

PHYSICS OF FLUIDS **27**, 013601 (2015)

Interaction between a laminar starting immersed micro-jet and a parallel wall

Juan Martin Cabaleiro,[1,a)] Cecilia Laborde,[2] and Guillermo Artana[1,b)]
[1]*CONICET-Fluid dynamics Laboratory, Faculty of Engineering, University of Buenos Aires, Av. Paseo Colón 850, Buenos Aires, Argentina*
[2]*Laboratory of Physiology and Molecular Biology, Exact and Nature Sciences Faculty, University of Buenos Aires, Buenos Aires, Argentina*

(Received 12 November 2013; accepted 11 December 2014; published online 6 January 2015)

In the present work, we study the starting transient of an immersed micro-jet in close vicinity to a solid wall parallel to its axis. The experiments concern laminar jets (Re < 200) issuing from a 100 μm internal tip diameter glass micro-pipette. The effect of the confinement was studied placing the micro-pipette at different distances from the wall. The characterization of the jet was carried out by visualizations on which the morphology of the vortex head and trajectories was analyzed. Numerical simulations were used as a complementary tool for the analysis. The jet remains stable for very long distances away from the tip allowing for a similarity analysis. The self-similar behavior of the starting jet has been studied in terms of the frontline position with time. A symmetric and a wall dominated regime could be identified. The starting jet in the wall type regime, and in the symmetric regime as well, develops a self-similar behavior that has a relative rapid loss of memory of the preceding condition of the flow. Scaling for both regimes are those that correspond to viscous dominated flows. © *2015 AIP Publishing LLC.* [http://dx.doi.org/10.1063/1.4905037]

I. INTRODUCTION

The dynamics of starting immersed jets have been widely studied in turbulent regimes due to their important role in different industrial applications such as fuel and oxidizer jets in combustion chambers, inkjet printers, or flow control, especially control of separated flows.

Laminar starting jets, however, have received less attention. Besides the academic interest, applications of similar flow configurations can be found in microfluidics. Instantaneous switching on of submerged laminar jets[1] can be used to perform analog or digital operations similar to those performed with electronics. Devices like fluid amplifiers are of interest in environments where electronic digital logic would be unreliable (e.g., in systems exposed to high levels of electromagnetic interference or ionizing radiation). In the domain of biology, these types of jets are used for instance as a stimulus to study the response of type T mechanic-sensorial receptors of the *Hirudo Medicinalis* leeches to shear stresses.[2] Laminar starting jets are also studied in relation to biological propulsion mechanisms.[3]

Jets of this kind can be characterized by the evolution of a vortex head and the jet stem formed between the nozzle and the structure.

At the first stage of the injection of the fluid in the quiescent environment, a vortex head is created due to the roll up of the vortex sheet that separates at the edge of the exit orifice. This structure grows rapidly in size by absorbing all of the fluid ejected from the nozzle and does not translate considerably while it remains attached to the nozzle. The initiation of the starting jet is characterized by the

a)jmcabaleiro@fi.uba.ar. Also at Micro and Nanofluidics and Plasma Laboratory, Faculty of Engineering, Marina Mercante University, Av. Rivadavia 2258, Buenos Aires, Argentina.
b)gartana@fi.uba.ar

separation of this vortex structure from the nozzle and the formation of a trailing jet behind the translating leading vortex head.

At very low Reynolds number, Cantwell[4] studied the starting process of round jets using an axisymmetric Stokes flow approximation and obtained the particle paths at Reynolds number $Re \leq 30$, based on the exit velocity U_0 and on the nozzle diameter D. He showed that when coordinates are scaled with the square root of time, the starting vortex becomes a self-similar flow.

Other theoretical studies have proposed models consisting of a spherical vortex head structure[5,6] or a Norbury vortex ring[7,8] interacting with a steady jet.

At relative high Reynolds number ($Re \sim 3000$), Gao *et al.*[9] have described a pinch-off process of the starting jet in which the vortex head detaches from the trailing jet at distances of $\sim 10D$. An adequate interruption of the fluid injection leads to the formation of an isolated vortex ring translating in the quiescent fluid by its self induced velocities. Vortex rings have been studied in depth since some of the early works of Helmholtz[10] and Reynolds.[11] In particular, vortex rings in unbounded semi-infinite domains are well understood, including the formation dynamics, their propagation, and transition to turbulence (see for instance Shariff and Leonard[12] or Lim and Nickels[13]).

When Reynolds numbers are moderate ($Re < 1000$), the leading vortex remains attached to the enlarging jet stem for long distances as long as the fluid continues discharging from the orifice. In this case, the toroidal vortex, which forms the jet head, grows in time by fluid entrainment directly from the surroundings as well as from the quasi-steady trailing jet structure.

The growing vortex head of the starting jet may travel with a rectilinear motion or with deviations from the axial direction. Deviations of the jet column are in general associated with the development of instabilities that alter the dynamics of the head.[14] In transient jets, Witze[15] and Ouellette and Hill[16] have shown that the fluid flow solution for the quasi-steady state jet is valid for the stem of the starting jet, even in the jet's initial stages of development. Therefore, it is likely that instabilities observed in steady jets should also be present in the starting jet.

The instabilities observed in steady axisymmetric jet flows are either of the sinuous kind: characterized by helical-spiral modes in which the waves associated with the instabilities appear as a rhythmic undulation or twisting of the jet, or of the varicose kind: characterized by axisymmetric modes in which the waves travel as a succession of symmetrical swellings and contractions. Increasing Re from 100 to 1000 in steady jets, Crow and Champagne[17] found a continuous evolution from helical to axisymmetric structures. The latter tend to prevail at larger values of Reynolds number. In Ref. 18, the critical Reynolds number for the onset of instabilities in a steady jet was found numerically to be close to 220. However, this value depends on different parameters of the simulated situation. It has been found that the assumed velocity profile influences the critical Reynolds number associated with the onset of instabilities. In particular, the boundary layer thickness, which would be different for a tube, a square-edged orifice or a knife-edge orifice, has been identified as an important criterion in the production of instabilities and promotion of the various structures. Also, because of the convectively unstable nature of the jet instabilities, the stochastic nature of surrounding disturbances becomes another significant aspect in the onset of the instability development process.[19,20] O'Neill *et al.*[21] found experimentally that for $Re < 500$, the instabilities of jets can be dampened at very long distances from the nozzle exit. The author concluded that the perception that steady round jets at low Reynolds numbers were unavoidably unstable flows, supported by previous flow visualization studies, was erroneous.

For laminar starting jets, Reynolds[22] found a variety of instabilities in the jet (pedal breakdown, sinuous oscillations, and shearing puffs) with onsets at very low values of the Reynolds number. These experiments are in contradiction with the results of Danaila *et al.*[18] or O'Neill *et al.*,[21] but as some works signal,[23] Reynolds' results, especially those for $Re < 150$, could have been seriously affected by the presence of appreciable background disturbances in the experimental apparatus.

The use of starting micro-jets enables studying starting jets that are less prone to develop instabilities. Gau *et al.*[24] and Aniskin *et al.*[25] have recently reported that steady micro-jets are more stable than large-scale jets. One possible explanation of this enhancement of stability can be associated with a low level of the background perturbations with short wavelengths (or high frequencies) that these jets would require to develop instabilities with a high growth rate.

The presence of a wall at close proximity to the starting jet may also affect the vortex structure of the head and the instabilities developed in the trailing jet. This is one of the subjects that we address in the present paper.

When a vortex filament is convected near a solid surface, a viscous response appears in the near-wall flow. For vortices with high enough values of circulations, a sequence of events initiates in the boundary layer, which culminates in an abrupt eruption of surface fluid and usually leads to the formation of a new vortex structure. In general, such eruptive events develop because a vortex in proximity to a wall induces a persistent adverse pressure gradient on the boundary layer and/or a local concentration of the vorticity field. Reports of the paradigmatic vortex ring interacting with solid bodies can be found for instance in Refs. 26–28. However, most of these studies involve a vortex ring impacting normally on a wall or with a wall at an angle with its direction of propagation. The motion and the structure of a vortex ring convecting in a quiescent fluid, parallel to a plane wall, were just recently described by O'Loughlin and Bohl.[29] The initial vortex ring trajectory was reported to divert towards the wall as described by an inviscid flow model. However, as the ring came closer to the wall, the interaction became viscous in nature and was qualitatively similar to that of a vortex ring/oblique wall interaction.

Other studies have also analyzed the effect of a radial confinement of laminar steady jets. For coaxial confinements,[30,31] the flow typically comprises a pair of symmetric vortices trapped between the jet like core flow and the downstream channel walls. With increasing jet velocity, a critical value of Reynolds number is reached at which the symmetric flow downstream of the jet exit breaks down into an asymmetric flow through a pitchfork bifurcation. In general, however, for $Re < 300$, coaxial confinement does not greatly affect the jet stability.

To the best of our knowledge, the present paper is the first study dealing with stable starting jets generated close to a plane rigid parallel wall. The study is undertaken with micro-jets originated through the end of a capillary tube with Reynolds number corresponding to the sub-critical regime ($40 < Re < 130$). The goal of our work is to analyze stable transient starting jets and to identify the effect of the wall on the flow. Moreover, we aim to experimentally determine its scaling laws.

The rest of the manuscript is organized in sections. First, we describe the experimental setup then the experimental results, describing the characteristics of the observed regimes. We then proceed to a discussion introducing both numerical simulation and scaling laws in order to unveil some of the underlying physics of this phenomenon. The results are summarized at the end of the manuscript.

II. EXPERIMENTAL ARRANGEMENT

To create the starting jet, we used glass capillaries (microcaps-Drummond, US) (inner diameter $D = 0.1$ mm, outer diameter $OD = 0.5$ mm, and length $L = 20$ mm) placed horizontally at the center of a distilled water-filled tank ($100 \times 50 \times 20$ mm).

A large number of studies dedicated to the study of vortex rings have considered the use of a piston driven mechanism to inject fluid in a quiescent media. For starting jets, other types of studies choose the sudden pressurization of a pipe system ended with a nozzle through the rapid opening of a solenoid valve. For micro-jets, a commercial system that enables the injection of very small amounts of fluid in a controlled way is available, and hence we chose this last option. The pipettes were therefore connected to a computer controlled pressure pulse generator Picospritzer II (Parker Corporation, General Valve Division, Fairfield, NJ) with tygon tubes (0.762 mm inner diameter and length of 500 mm). The system generated the jet by imposing a pressure step into the tube filled with water, colored with methylene blue.

By recording the position as a function of time of the liquid-gas interface inside the tygon tube with a video camera, it is possible to obtain a picture of the typical transient of the flow rate injected by the system. In Fig. 1, we show the dynamics of the meniscus during the opening and closure in a shortened experiment for three different pressures. We can observe during the start phase, an initial increase of the meniscus velocity until a peak value followed by a decrease to an almost constant value. During the stop phase, it can be observed that the meniscus not only decreases its velocity but it also has a backward displacement. In this work, we undertook longer experiments (~1 s) and focused

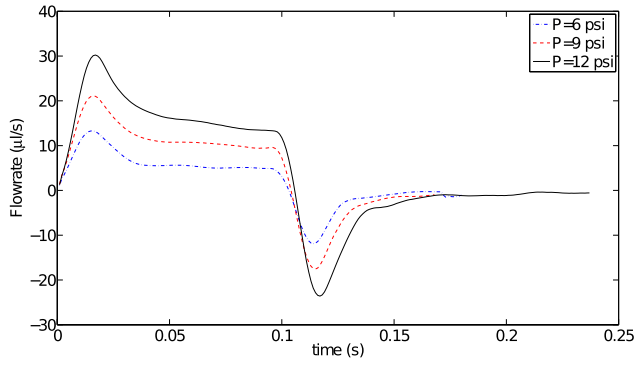

FIG. 1. Typical initial transient of the flow rate as a function of time at three different pressures. Opening and closing of the solenoid valve.

our analysis on the long term dynamics when the steady regime is well established. As we will show, the initial transient, even of large importance for studies related to vortex ring dynamics or related to initial stages of jet flow, seems not to significantly alter the characteristics of the long term dynamics of the jet flow.

It is worthy to mention that because of the way we have performed the measurement, the peak value of the flow rate during the initial transient may result overestimated when directly read from this graph. Indeed, when the valve is opened (closed), a dilatation (contraction) of the tygon tubing is expected. Thus, for the very first stages of the experiments and for those occurring after the closure, the tracking of the movement of the interface cannot be directly associated with the real value of the mean exit velocity from the nozzle. It is however possible to propose a rough correction to the measurements for the initial transient. To this end, we can compensate the excess in the measurement during the initial stage when values of the flowrate are contaminated by the expansion of the tubing and by subtracting the values associated with the receding meniscus phase, which are associated with the contraction of the tubing. The corrected transient obtained by this procedure can be observed in Fig. 2. In this figure, it is possible to visualize that after a time lag of 10 ms, the flow initiates, attains a peak value, and then decreases to an almost constant value. The compensated peak values are much smaller than the ones observed in the uncompensated case. Under these considerations, we can state that volumes dispensed by the system are linear over time, with a short transient to attain constant volume flow rate (~50 ms). Finally, we can also signal that Abramovich[5] undertook experiments of a starting jet by a sudden opening of a valve, and the pressure recordings over time show a behavior that is consistent with the evolution of the flow rate of our experiments.

A glass wall in horizontal (Fig. 3(b)) or vertical (Fig. 3(c)) position was placed parallel to the jet axis to enable lateral and top views of the flow patterns. The relative position of the pipette to the wall was varied by means of a micromanipulator (Narishige, Japan). The angle formed between

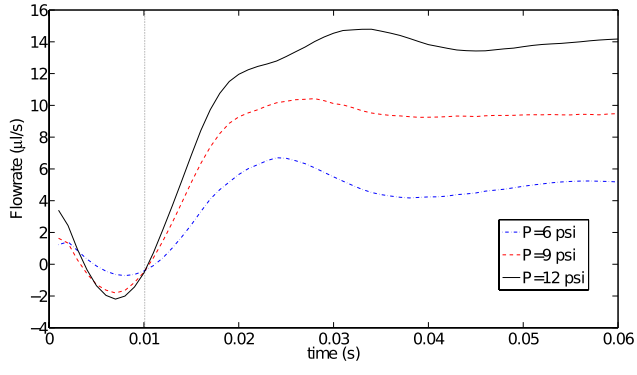

FIG. 2. Corrected initial transient of the flow rate as a function of time at three different pressures. Opening of the solenoid valve.

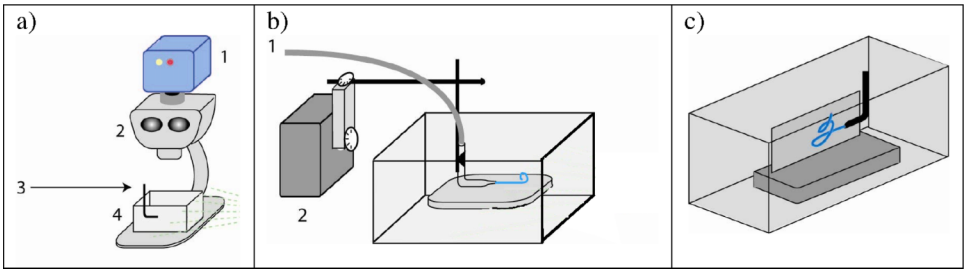

FIG. 3. (a) 1-High speed digital camera. 2-Stereoscopic microscope. 3-Connection to pressure pulse generator. 4-PMMA chamber and micropipette. (b) Wall position for top view recording. (c) Wall position for lateral view recording.

the jet axis and the normal to the wall surface was 90° ± 1°. Four different pressure values were set in the apparatus to generate jets with different Reynolds numbers in the range of 40–130. Flow rate plots like the one shown in Fig. 2 were obtained for each pressure value. The flow rate corresponding to the different pressure steps was taken as the plateau flow rate in those plots. The starting jet was visualized through a trinocular stereozoom microscope Olympus SZ60 (Olympus, Japan) using two different magnifications. The pictures obtained were images of 512 × 512 pixels recorded at 300 and 600 frames per second with a digital Cmos fast camera SpeedCamMiniVis (Weinberger, Germany). Image scales were determined from a reference grid. The original images were post-processed by subtracting the background image and increasing the contrast. During the first stages of this research, the light source was located at the side of the stereozoom microscope, in line with the jet's axis, at an angle of about 45° from the horizontal plane. This illumination produced the shadows that can be seen in Fig. 4. Subsequent images were obtained using a led ring illuminator, which corrected for this shadowing effect (Fig. 5).

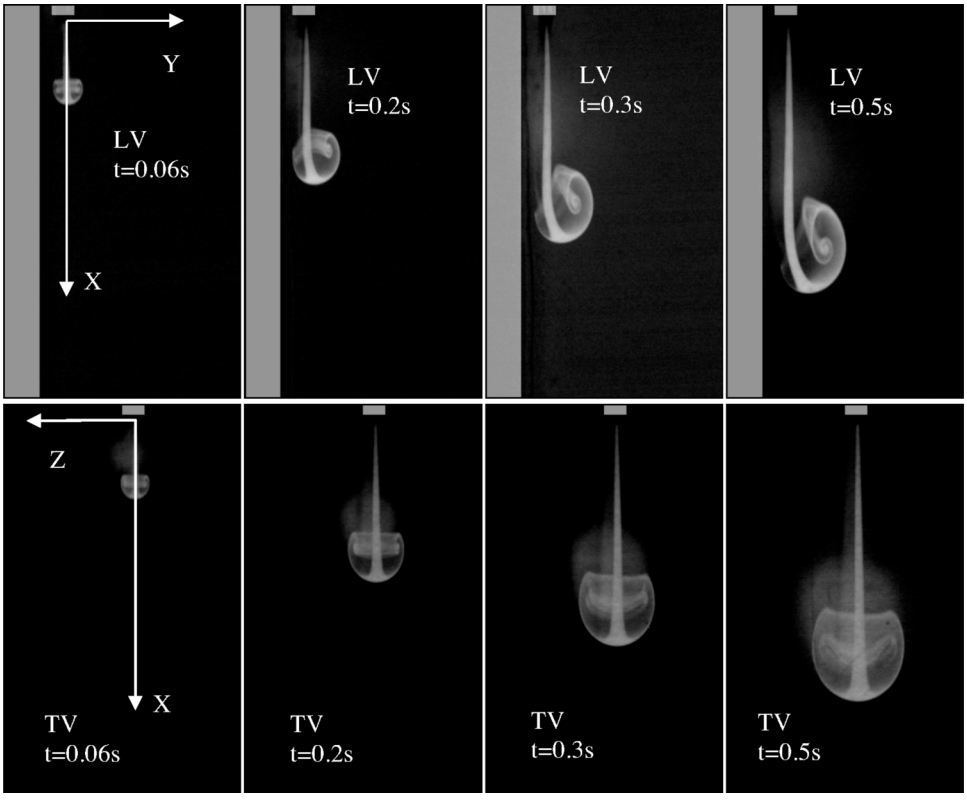

FIG. 4. Top figures: LV and bottom figures: TV of a jet at $Re \sim 50$ at four different times. The first (left, LV and TV) images correspond to the regimen with axial symmetry (symmetric regime). The last (right, LV and TV) images correspond to the wall regime. The coordinate system is drawn in the first top view and in the first lateral view.

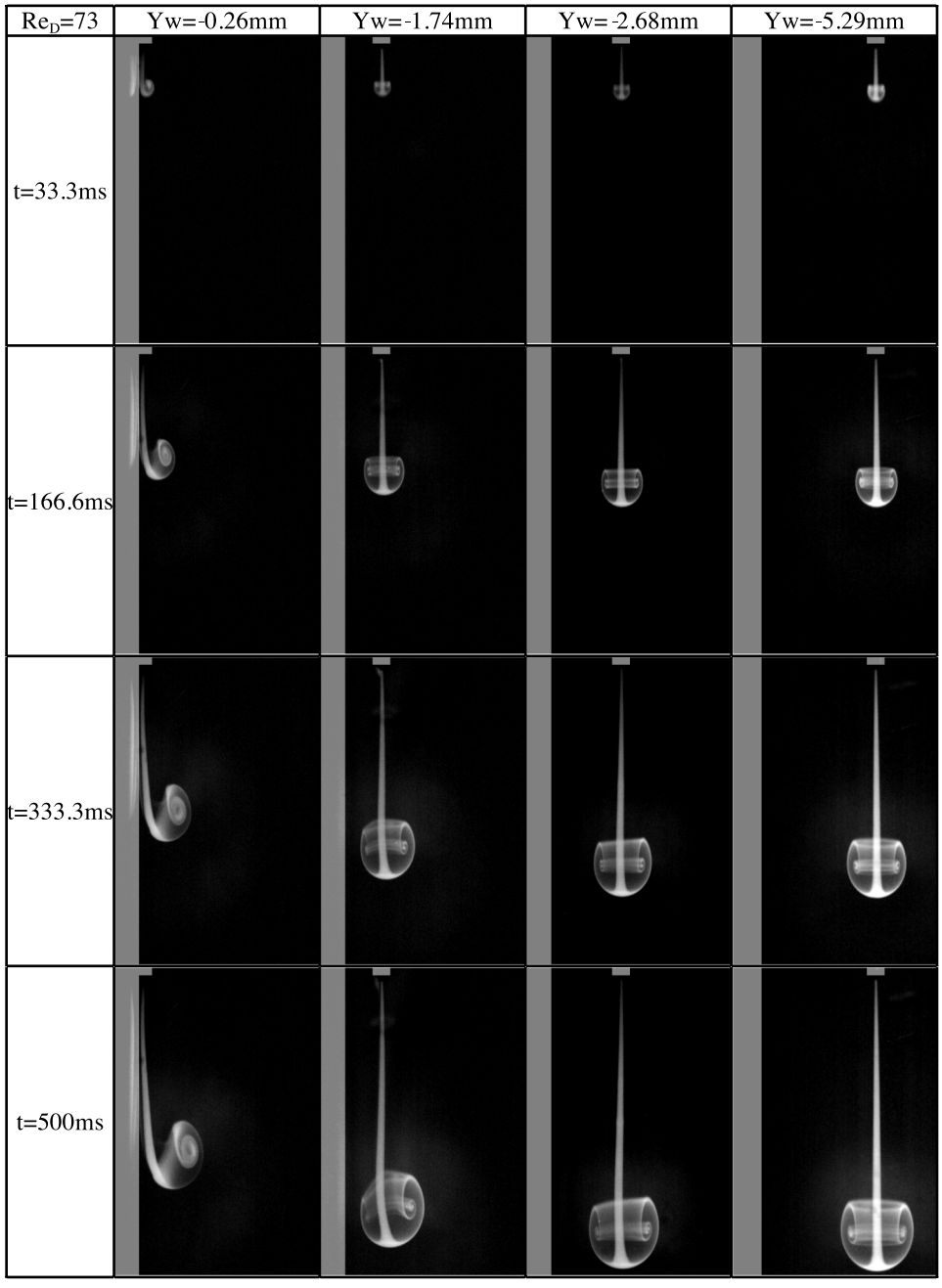

FIG. 5. Lateral views at $Re = 73$ at different distances from the wall. From left to right: 0.26, 1.74, 2.68, and 5.29 mm.

After each experiment, the water in the tank was allowed to come to rest by waiting 30 minutes before starting a new experiment.

III. EXPERIMENTAL RESULTS

In Fig. 4, we show visualizations of the flow patterns with top (TV) and lateral (LV) views for a typical case ($Re \sim 50$ and non-dimensional distance to the wall $Y_W/D \sim 6$) at different times. As the jet develops, different flow configurations appear. In the symmetric regime (Fig. 4, left, LV and TV), the vortex head is formed, separates from the nozzle and travels in the fluid in the axial direction keeping

its axial symmetry. In our experiments, the formation process of the head is very short ($t \sim 10$ ms) compared to other time scales. The head continues to increase in size and the jet column is conical, with an axis that remains rectilinear all along the symmetric regime. In the wall regime (Fig. 4, right, LV and TV), the axial symmetry of the head is lost. The head tilts and it starts moving first towards the wall and then away from the wall. The vortex head evolves not only in size but also in shape during this stage. The axis of the jet column is no longer rectilinear.

In this regime, the LV show that the presence of the wall breaks the symmetry of the streaklines. However, the TV show that the symmetry of the streaklines with respect to the midplane is not altered by the presence of the wall. Figure 5 shows LV for a jet of $Re = 73$ at different distances from the wall. It is clear that the further the jet is located from the wall, the later the last two scenarios described above occur.

A. Symmetric regime

In this regime, the jet patterns are quite similar to those of the start-up of a laminar free jet flow. Once the vortex head is formed and separated from the nozzle, the structure remains axisymmetric and grows with time. The lateral and top views are therefore almost identical.

A schematic representation of the head of the liquid emanated from the nozzle is displayed in Fig. 6(b), in the mid plane perpendicular to the wall surface and containing the jet axis. Two symmetric spiraled vortices with *vortex centers* at positions $(R_V, 0, X_V)$ and (R_V, π, X_V) appear in the midplane (positions are measured in a cylindrical coordinate system, R_V is the radial position of the vortex center and X_V is the axial position of the vortex center) and are located at an axial distance $(X_F - X_V)$ from the axial position of the *front* point (X_F, the part of the head with the largest value of the axial coordinate x at a given time). It is important to mention that this is a definition, and that these coordinates do not coincide with the local maxima of the vorticity field. We can also consider the *top* and *bottom* points of the head ($(Y_U, 0, X_U)$ and (Y_L, π, X_L)). The positions of these last two points coincide with the points exhibiting the largest radial coordinate in which the tracer can be detected. Because of the existing symmetry, $X_U = X_L$ and $Y_U = Y_L$.

The *front*, *vortex centers*, and *top* or *bottom* points of the vortex do not move together with the same velocity. In the present regime, the velocity of the *front* has only one component that agrees with the axial direction, and there is no deflection of the *front* trajectory from the jet axis.

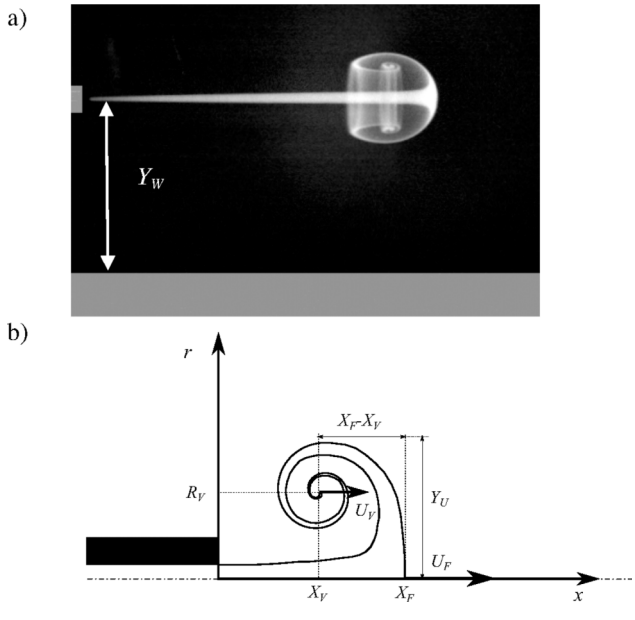

FIG. 6. (a) Lateral view of symmetric phase. (b) Schematic of the vortex head with notation.

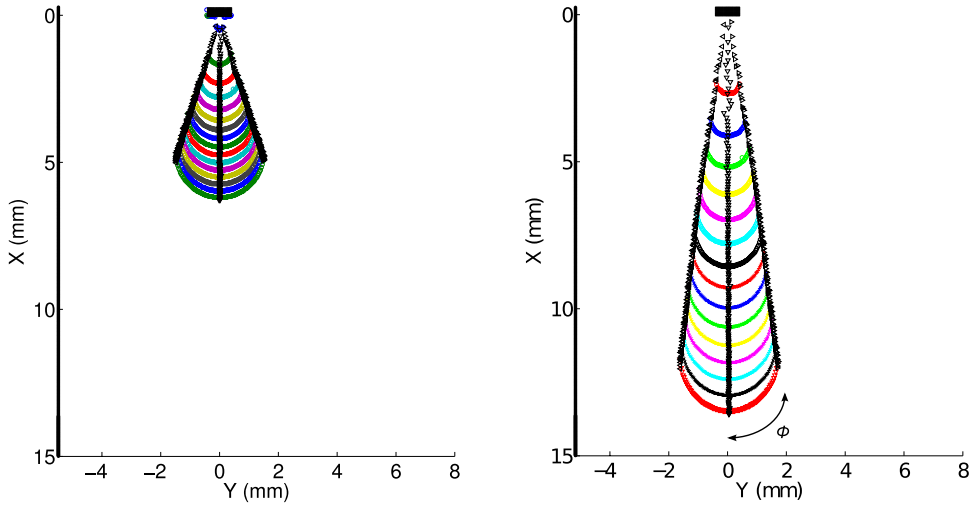

FIG. 7. Frontlines from the coordinate system of Fig. 4. Frontlines sequences are constructed considering time steps of 33.3 ms starting at 33.3 ms. Left: $Re = 40$; $d = 5.4$ mm. Right: $Re = 73$; $d = 5.4$ mm.

On the contrary, the *vortex centers*, *top*, and *bottom* points have an axial and a vertical velocity. From visualization experiments, it is cumbersome to determine the position of the *vortex centers*. Hence, it is convenient to restrict the analysis to the evolution of the *front*, *top*, and *bottom* points.

1. Frontlines

It is possible to represent the frontline positions at different times. This line is formed at different times by the points with the largest radial coordinate in which the tracer can be detected (measured from a polar coordinate system placed at the jet origin). We show in Fig. 7 a typical time series of the frontline for this regime.

As shown by these figures, in this regime, the top and bottom points separate from each other forming an almost constant angle (ϕ) with respect to the centerline, that is a function of jet's exit velocity. The symmetry observed indicates that there is not an appreciable effect of the wall.

We represent in Fig. 8, the tangent of the angle for different Reynolds numbers. The angle in this regime decreases with the jet's exit velocity, and a good fit is obtained with a Boltzmann type function.

2. Front and lateral point velocities

Prandtl's[32] analysis of a starting jet was revisited recently by Hettel *et al.*[33] using Bernoulli's equation applied to the axial streamline. It was found that the velocity of the front (U_F) was constant and could be related to the jet's exit velocity (U_0) by the expression $U_F/U_0 = 0.5$.

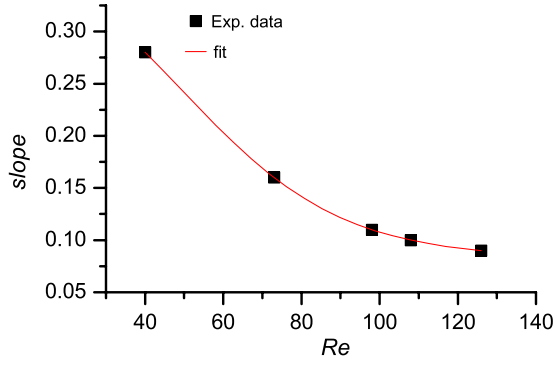

FIG. 8. Tangent of the angle formed by the frontlines in the symmetric phase for different Reynolds numbers.

Hettel *et al.*[33] verified this relationship numerically considering a velocity U_0 related to the velocity of a piston that pushed the fluid through the nozzle. This expression was tested for short distances of the vortex head from the nozzle exit (about 3 diameters). When considering larger distances, this expression is inadequate. The local value of the jet velocity should be taken into account instead of the one at the nozzle exit.

For a steady laminar jet, it was proved[34] that in the axis of the jet issuing from a point source, the local velocity is inversely proportional to the nozzle exit distance x: $U_0 \sim K/x$. Here, x, y, z is a Cartesian coordinate system (Fig. 4), and K is Landau's constant.

Based on Cantwell's[4] study (which extended this analysis to the case of a starting jet), the *front* velocity can be expected to follow the same dependence with respect to the axial coordinate. In many cases, however it has been convenient to modify this law and consider that the jet origin is slightly displaced from the nozzle exit (virtual origin of the jet). On this basis, a velocity fit of the front can be proposed with an expression of the type

$$U_F = \frac{K}{2(x - X_0)}. \tag{1}$$

Here, we introduce a virtual origin of the jet through X_0, as done in several works. To describe the trajectory of the front, a power law of the following type can be proposed

$$X_F = a(t - t_0)^b + X_0. \tag{2}$$

The time t_0 can be associated with the vortex head formation time[3] prior to its separation from the nozzle. Taking into account, this expression it follows that

$$U_F = ba^{\frac{1}{b}}(X_F - X_0)^{\frac{b-1}{b}}. \tag{3}$$

When $b = 1/2$, the dependence of the front velocity with the axial coordinate stated by Landau's expression is recovered. K in Landau's expression is then equal to a^2.

Power-laws were fitted to the front position curves shown in Fig. 9 at different Reynolds numbers. Note that in these figures, we have represented the square root of time as the abscissa. In agreement with the observed alignment of points along straight lines, the coefficient b obtained with these fits appears to be a constant value of 0.5 in all our experiments. The virtual origin on the other hand increases with the jet's exit velocity (Fig. 10) but no clear effect of the wall distance was observed.

With the value of $b = 1/2$, it is possible to define a nondimensional number

$$Re_F = \frac{U_F(X_F - X_0)}{\nu} = \frac{a^2}{2\nu}. \tag{4}$$

This local Reynolds number based on the *front* axial position and the *front* velocity can be used to characterize the flow in this regime, and it remains constant when times considered exceed the transient to attain a constant flow rate.

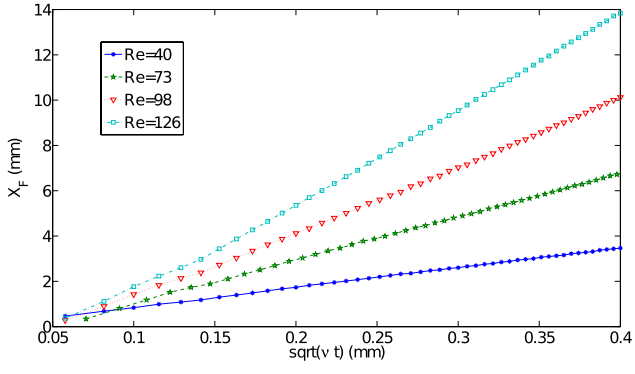

FIG. 9. Horizontal position of the front X_F as a function of the square root of time t. Jet flowing at different Reynolds numbers. Nozzle axis placed at a distance of 5.4 mm from the wall.

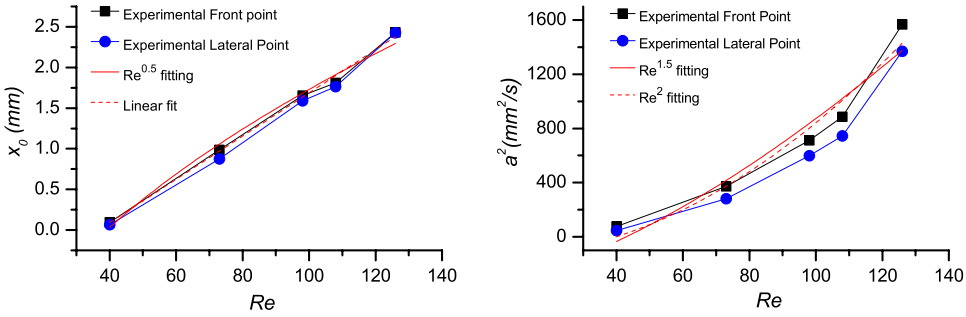

FIG. 10. Left: Virtual origin of the jet considering the front point position and the lateral point positions as a function of Reynolds number. Right: Coefficient a^2 of Eq. (2). Solid lines correspond with Abramovich's[5] fit of the *front* point. Dashed lines correspond with Andrade and Tsien's[35] fit of the *front* point.

In steady jets, Abramovich[5] obtained that the empirical value of the constant K was proportional to $Re^{3/2}$ (Re based on the nozzle diameter and the jet's exit velocity), while Andrade and Tsien[35] found it was proportional to Re^2. Both Cantwell[4] and Prandtl[32] analyzed the case of a jet produced by a constant force directed along the x-axis immersed in an infinite domain. According to their work, it is expected that, for short distances from the jet origin, the constant K (for starting jets) can be determined by the following law:

$$K = \frac{8\nu}{A-1}, \tag{5}$$

where ν is the kinematic viscosity, A is a constant, and

$$\frac{{Re_J}^2}{16\pi} = A + \frac{4}{3}\frac{A}{A^2-1} - \frac{A^2}{2}\ln\left(\frac{A+1}{A-1}\right). \tag{6}$$

Here, a Reynolds number Re_J has been defined in terms of the amplitude J of the force directed along the x-axis and the density of the fluid ρ

$$Re_J = \frac{J/\rho}{\nu}. \tag{7}$$

For $Re_J >> 1$, the use of Eqs. (5)–(7) indicates that the constant should behave like $K \propto {Re_J}^2$. We show in Fig. 10, fits of the virtual origin and of coefficient a^2 for different Reynolds numbers. We indicate in the graphs the fits with the Reynolds dependence observed by Abramovich,[5] and by Andrade and Tsien.[35] The expected quadratic dependence of K (or a^2) with respect to the Reynolds number does not seem appropriate in our case. A better fit is obtained with $Re^{2.5}$. Different factors may play an important role in explaining the discrepancies with theoretical results. For instance, the finite size of the tank that is considered, or the fact that the force is generated by a finite-diameter jet-tube.

The power laws postulated for the front point positions over time stated by Eq. (2) may also be proposed for the lateral points. A square root dependency of the position of the lateral points' position over time is again observed. In Fig. 10, we also show the values of the coefficients of the power laws for the lateral points (with $b = 1/2$). As these graphs show the constant affecting the square root of time is different for the lateral and the front positions. This means that the front and the lateral velocities are different at the same time. Lateral points are retarded with respect to the front point.

3. Vortex head diameter

The jet feeds fluid into the spiraled vortex accompanied by an entrainment of the surrounding media that produces, as a result, an increase in size of structures over time. In the symmetric regime, this process can be characterized considering a characteristic diameter $D_H = R_U + R_L$. In our experiments, D_H grows with time. The curves of D_H can be fitted with the following expression:

$$D_H = A_1 t^{B_1} - C_1. \tag{8}$$

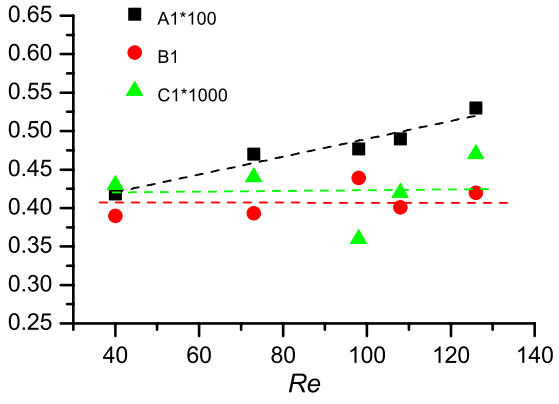

FIG. 11. Constants for the increase of the vortex diameter (Eq. (8)) as a function of Reynolds number.

We show in Fig. 11 the values of the coefficients of Eq. (8) for the different experiments. The values of B_1 and C_1 seem to be almost constant (close to 0.4 and 0.000 42, respectively), whereas the value of A_1 seems to be linear with Re. Gao *et al.*[9] found that after a short time of initiation of injection, the vortex ring diameter grew as a linear function of time. In the simulations of a starting free laminar jet, Hettel *et al.*[33] observed that close to the nozzle the volume of the head increased linearly with time, assuming that the head was a perfect torus. However, these calculations remain valid only for very short times after initiation as no entrainment of surrounding fluid was considered. Therefore, it is inadequate to extrapolate these results to our experiments. In our experiments, we observed that in the range of times corresponding to the symmetric regime, D_H grows with a power of time that remains close to the value of 0.4.

B. Wall dominated regime

In the wall dominated regime, the vortex head and jet column are clearly altered by the wall presence (Fig. 12).

The initiation of the transitional regime can be linked to the increase of the vortex head size. An upper bound of the time required for the wall dominated regime's initiation can be related to the time required by the vortex head to attain dimensions that become comparable with the wall-nozzle axis distance $d = -Y_W$. We can make use of the curve fits of the symmetric phase to give an upper bound of this time T_{max}, considering as limiting value $D_H/2 = d$

$$T_{max} = \left(\frac{d + C_1}{A_1}\right)^{\frac{1}{B_1}}. \tag{9}$$

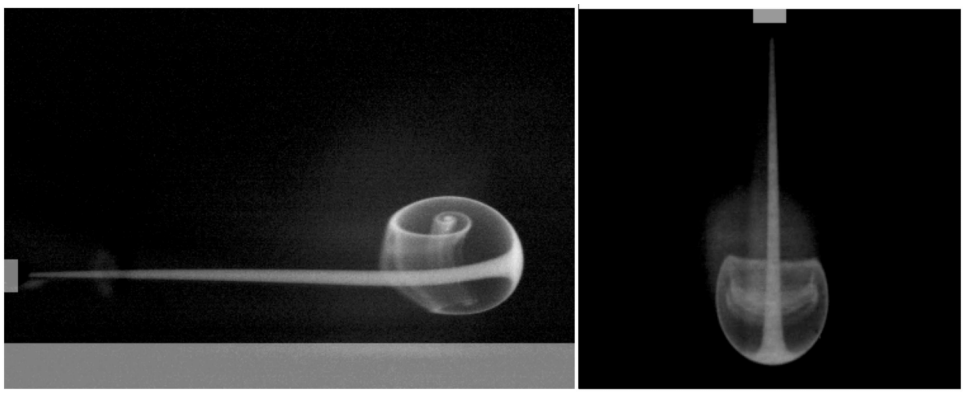

FIG. 12. Visualization of the first stages of the Wall regime. Left: Lateral view. Right: Top view.

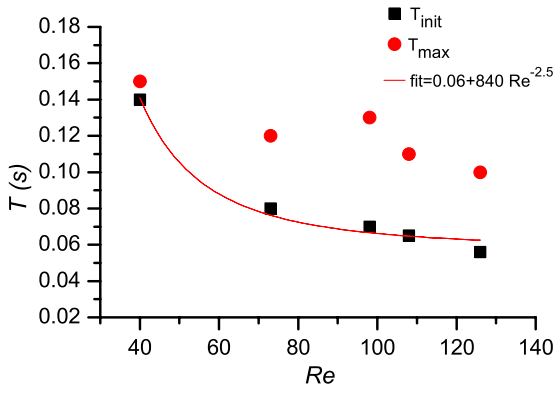

FIG. 13. Time required for initiation of the wall regime. Nozzle distance to the wall $d = -Y_W = 1.6$ mm.

In order to quantify the initiation of the transitional stage, we compare for each experiment the values of Y_L and Y_U at different times. Comparing the values of Y_L vs. Y_U, we define the initiation time of the regime T_{init} as the one corresponding to the separation of experimental points from the slope 1 by 5%. Fig. 13 shows these values. For a given distance to the wall and taking into account our data, it is expected that this time will decrease following a law proportional to $Re^{-2.5}$. The value of T_{max} overestimates the beginning of the regime but remains a good first approximation.

1. Head trajectory and velocities

In Fig. 14, we represent typical trajectories of the *front*, *top*, and *bottom* points of the jet during the wall regime. The head trajectory is initially almost rectilinear but during the roll-up of the vortex ring, it moves away from the wall. As a consequence of the vertical movement of the head, the streak-line of the axis of the jet stem does not remain rectilinear any longer and bends, first approaching the wall and then separating from it (Fig. 12).

Typical frontlines for the wall dominated regime at different times are given in Fig. 15. As we can observe the rectilinear movement of the front is lost and we can no longer identify symmetry around the centerline.

In Fig. 16, we show the horizontal position of the front versus the square root of time. We represent cases at two different distances from the wall. At the larger distance, the wall regime does not take place and, therefore, the results enable comparison with the symmetric regime. The comparison shows that proximity of the wall to the vortex head decreases the horizontal velocity of the front.

For the field of view of the experiments, the vertical velocity of the front increases with time until attaining an almost constant value. Note that in Fig. 17, a constant velocity is represented as the square of the abscissa.

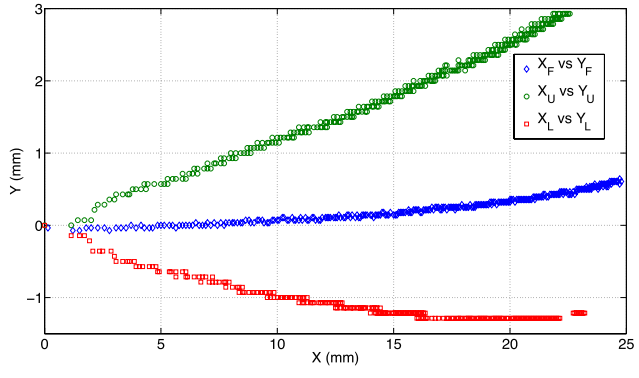

FIG. 14. Trajectories of the *front*, *top*, and *bottom* points of a jet at $Re = 98$ and $Y_W = -2.3$ mm.

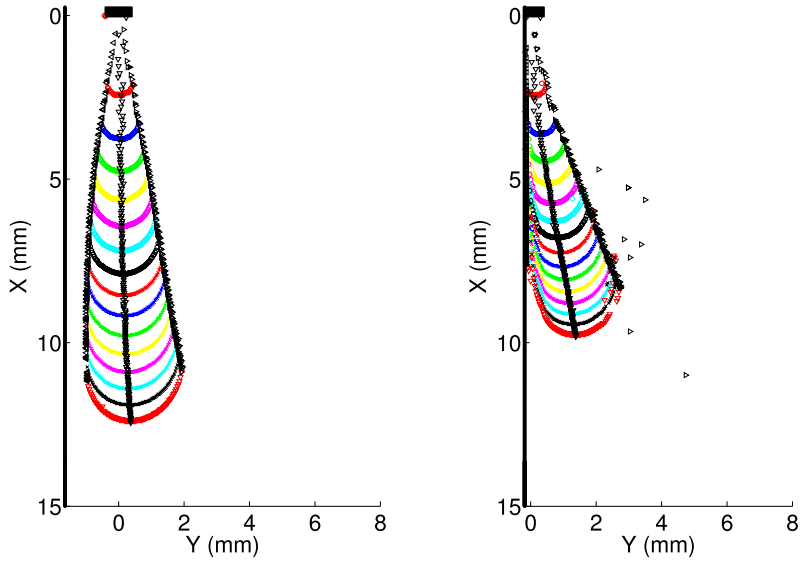

FIG. 15. Frontlines from the coordinate system of Fig. 4 considering time steps of 33.3 ms starting at 33.3 ms. (a) $Re = 73$; $d = 1.6$ mm; (b) $Re = 73$; $d = 0.26$ mm.

It was observed that this quasi steady velocity increases with Reynolds number and, for a fixed value of Re, it decreases as the distance to the wall increases (see Fig. 18, note that in these plots, the vertical velocity is normalized with the jet's exit velocity). In our experiments, Re number variations were achieved by changing the jet's exit velocity. Therefore, an almost constant value of U_y/U_0 (as in Fig. 18, left) indicates a linear increase of the vertical velocity with Re.

IV. DISCUSSION

In order to better understand the underlying physics of the starting jet, and of the influence of a wall placed at close proximity to it, we proceeded to analyze the problem through the use of non-dimensionalization and scaling. Numerical simulations were also carried out to complete the analysis.

When the governing equations and boundary conditions (BCs) of a problem are invariant under a Lie's group, the solution is also invariant under the same group. In this case, the solution can be expressed in terms of a reduced set of combinations of the basic variables, called the similarity variables. The fundamental one-parameter (s) dilation group can be expressed as

$$\breve{r} = e^s r; \quad \breve{\theta} = \theta; \quad \breve{t} = e^{2s} t; \quad \breve{u^i} = e^{-s} u^i; \quad \breve{p} = e^{-2s} p, \tag{10}$$

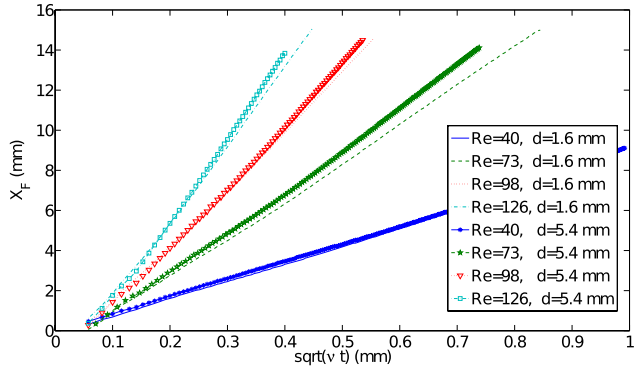

FIG. 16. Nondimensional horizontal front position as a function of the square root of time. Starting jet at different Reynolds numbers (40, 73, 98, and 126) and two nozzle-wall distances.

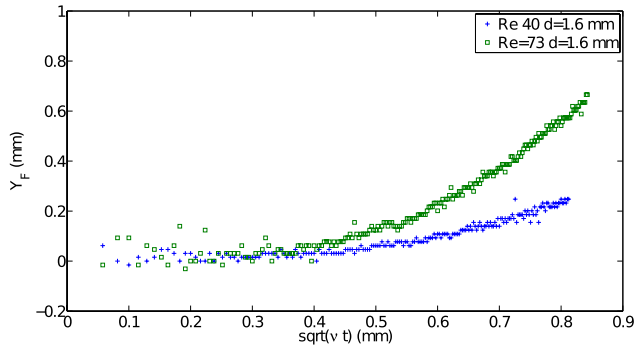

FIG. 17. Nondimensional vertical front position as a function of the square root of time. Starting jet at two different Reynolds numbers and a fixed nozzle-wall distance.

where r and θ are Polar coordinates, u^i are the velocity components in a polar coordinate system, p is the pressure, t is the time, $\breve{r}$ and $\breve{\theta}$ are the transformed polar coordinates, $\breve{u}^i$ are the transformed velocity components, $\breve{p}$ is the transformed pressure, and $\breve{t}$ is the transformed time.

The problem of the starting vortex formation in an impulsive started jet is invariant under the fundamental dilation group of the Navier-Stokes equation when the assumption of an unbounded flow produced by a force acting at the origin can be accepted.[4] Then, the unsteady flow dynamics of the jet can be analyzed in terms of the portraits of particle paths in similarity coordinates $x/sqrt(vt)$ and $y/sqrt(vt)$. The value of the parameter s is in this case 0.5. We will restrict our analysis of similarity to a single plane. In the symmetric regime, this is enough as we can take advantage of the axial symmetry of the flow. In the case of wall jet, we will consider the dynamics in the vertical plane of symmetry. This last option is not completely original for nonaxis-symmetric jets as similarity analysis restricted to planes of symmetry of the flows for the case of pulsating jets has been previously reported.[36] We concentrate our analysis mainly on the frontline dynamics as we can identify this line easily in the portrait of particle paths. As we mentioned before, our experimental study will be complemented now by the results issued from numerical simulations. Having all the variables available, this will help to unveil some of the underlying physics and illuminate our discussion. On the other hand, this approach will give us the opportunity to undertake a parametric analysis that would be more arduous to be done from physical experiments. The code used in the Computational Fluid Dynamics (CFD) study is Code_Saturne[37] and we considered both 2D simulations for the axisymmetric regime and 3D simulations for the study of wall regime. Details of the simulation domain and BC considered can be seen in Fig. 19. At the walls, Neumann BC was imposed to the pressure and Dirichlet BC to the velocity components, and at the free inlet/outlets, Neumann BC were imposed to the velocity components and Dirichlet BC to the pressure. At the symmetry plane, Neumann BC was imposed both to the velocity components and to the pressure. Given the symmetry observed from the top view in our experimental visualizations, we chose to use a half domain for the 3D simulations in order to reduce the number

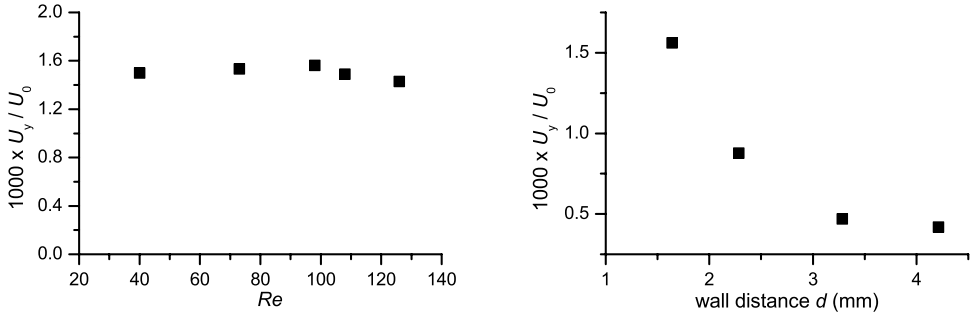

FIG. 18. Vertical velocity of the *front* point of the vortex head as a function of Reynolds number at $d = 5.4$ mm (left) and as a function of the distance to the wall (right) for a jet at $Re = 98$.

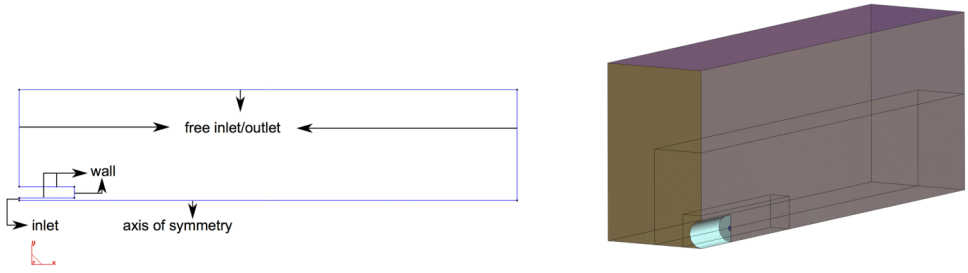

FIG. 19. Numerical simulations domains and boundary conditions. (a) 2D simulations; (b) 3D simulations.

of cells: we used a 3 million volumes non-uniform structured mesh, which was refined near the shear layer regions for these Direct Numerical Simulations (the smallest finite volume had a characteristic size of $0.02D$). Both the axisymmetric simulations and the 3D simulations were run in nondimensional form (the nondimensionalization parameters were the jet's exit velocity U_0, the fluid density ρ, and the orifice diameter D). The domain was 80 diameters long, 10 diameters wide, and 20 diameters high. The nondimensional time step for the simulations was 0.05. Smaller time steps were tested and no difference was observed between the solutions. Typical results of this kind of simulations can be observed in Fig. 20.

A. Symmetric regime

We consider here the early times of the flow and assume that the wall can be regarded as infinitely far away. We would like to signal three aspects that may break the dilation group invariance of the problem in our experiments. The first one is that the jet is not produced by a force but by the exit of a flow through an orifice. On one hand, this changes the problem because the momentum is incorporated to the fluid accompanied by a mass addition. Taking into account the work of Kurdyumov,[38] it is expected that this would require us to incorporate some corrective terms to the self-similar solution. Even if this correction would be small, the exit of fluid from an orifice incorporates a characteristic length of the problem (the radius of the jet at the exit orifice) that is absent when it is assumed that the jet is produced by a force. The second aspect that we also would like to highlight is the effect of the wall of the tube as a boundary that could alter the development of regions of self-similarity. The third aspect is related to the impulsional establishment of the flow and how this transient may alter the results.

We recall here the main results obtained by Sozou[39] and Cantwell[4] of a creeping unsteady jet. Taking into account the stream functions and particle path equation appearing in these works, it is possible to construct the phase portraits and a typical one can be observed in Fig. 21.

Cantwell[4] has signaled that the results issued from his model differed from numerical experiments of starting jets. He observed as main differences the long slender stem and a small angle of spread in the nonlinear high Reynolds number. We show in Fig. 22, our experimental results of frontlines in terms of the similarity variables $x/sqrt(\nu t)$ and $y/sqrt(\nu t)$. The cases illustrated correspond to situations in which the nozzle was placed at relative long distance to the wall.

As it can be observed, these graphs show that the transition to a self-similar behavior depends on the Reynolds number. At the relative low Reynolds number tests (Fig. 22, left), the self-similar

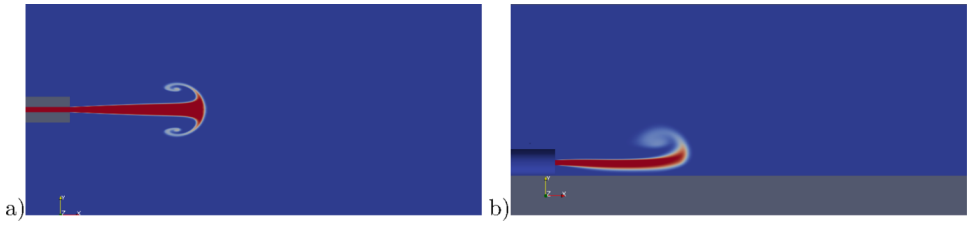

FIG. 20. Numerical simulations. Tracer concentration at $Re = 40$. (a) Early stages of the flow at large nozzle-wall distance (2D axisymmetric simulation) ; (b) wall regime, small nozzle-wall distance (3D simulation).

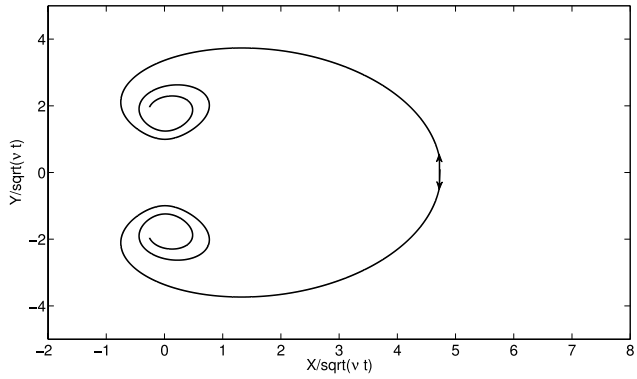

FIG. 21. Phase portrait in similarity variables of particle paths under a creeping flow assumption.[4] Force acting on x direction at the origin.

behavior occurs quite close to the origin. The collapse observed in this graph indicates that for the range of times observed, all the possible sources that could break the invariance of the problem and thus invalidate the self-similar behavior are not relevant. At larger Reynolds number (Fig. 22, right), the behavior is different, and in this coordinate system, the frontline occupies different positions until a collapse of the curves is attained. Thus, the self-similar region is found preceded by an initial transition region. Note however that the lateral points (bottom and top) tend to collapse quickly in a single y similarity coordinate but its x position and also the front point position require larger times.

The discrepancies, already observed by Cantwell,[4] between theory, and results obtained from numerical simulation of a jet flow produced by an impulsive force, are also present in our results concerning a jet flow produced through fluid injection. One can evaluate these differences considering the position of the front and top and bottom points in the similarity coordinates portrait once self-similar behavior is achieved.

We show in Fig. 23, the predictions of the front and lateral points that arise for creeping flows as Cantwell[4] considered. In his approach, he considered a Reynolds number defined in terms of the force applied at the origin Re_J. However, an equivalence with Re is immediate considering the momentum

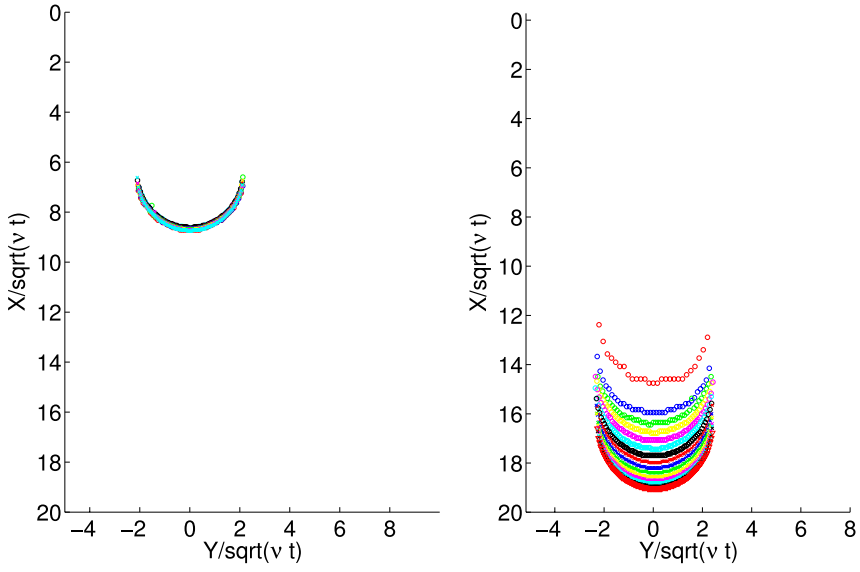

FIG. 22. Frontlines in terms of the similarity variables. Frontlines sequences are constructed considering time steps of 33.3 ms starting at 33.3 ms. Left: $Re = 40$; $d = 5.4$ mm. Right: $Re = 73$; $d = 5.4$ mm (symbols agree with those of Figure 7).

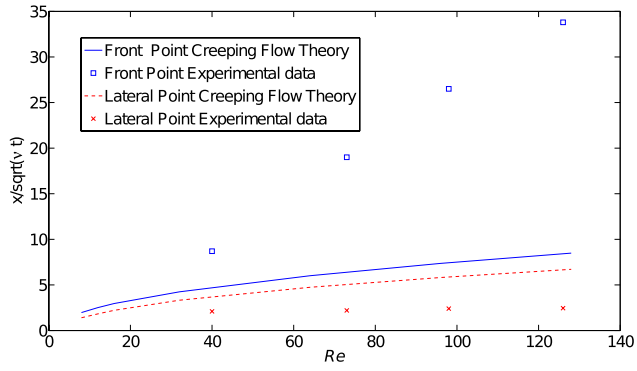

FIG. 23. Front position and maximum Y coordinate as a function of Reynolds number in the portrait phase diagrams. Values predicted under a creeping flow assumption[4] and experimental values.

flux imposed by the fluid injection to the quiescent liquid with the jet. As we can see from this figure, the position of the front point in the similarity coordinates increases with Reynolds number. The influence of Reynolds number on the position of the lateral point, and thus on the radius of the starting vortex structure, is much lower. Considering the assumption of creeping, a theoretical angle of spread can be deduced. This value is quite constant, close to 0.75, but contrary to what is observed in Fig. 8, it slightly increases with Reynolds number.

1. *Influence of the transient injection and nozzle wall thickness*

We would like to consider here the influence on the frontlines of the characteristics of the ramp imposing the flowrate and of the thickness of the nozzle wall. To this end, we have analyzed the results of 2D and 3D numerical simulations.

In a first study, for a given value of steady flow rate, we have considered different initial transients and analyzed the long term dynamics. 2D simulations were performed with four ramps similar to the ones observed in our experiments. The ramps were described by an exponential function that grows asymptotically in time to the steady value of the flow rate as

$$\frac{U(t)}{U_0} = 1 - exp\left(\frac{-t}{\tau}\right). \tag{11}$$

We have considered cases with the same value of U_0 and different time constants τ (1.4, 6.8, 27.4, and 109.6 ms) (see Fig. 24). The results obtained from the numerical simulations with the different ramps show that in all cases the behaviors at long term are alike to those of the experimental results (Fig. 25). In all cases, we observe a region where curves tend to collapse preceded by an initial

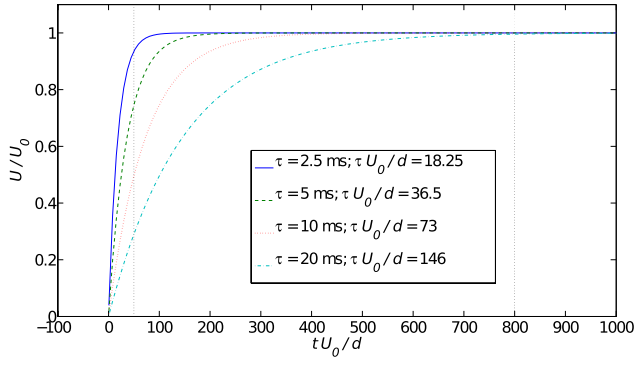

FIG. 24. Mean velocity ramps considered for the numerical simulations. The dotted lines mark the nondimensional times at which the tracer is represented in Fig. 25.

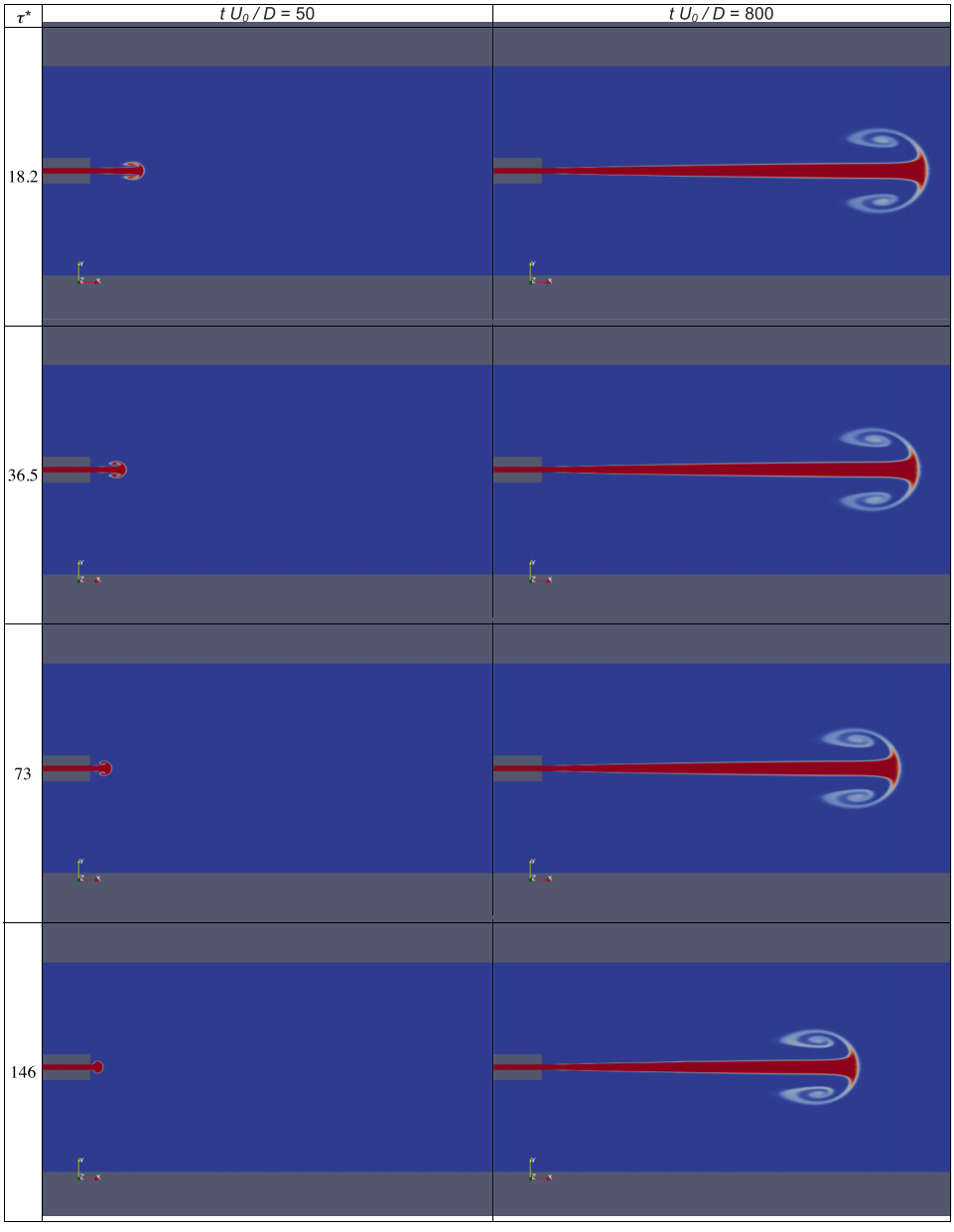

FIG. 25. 2D Numerical simulations to illustrate effect of time constant τ of the velocity ramp. Tracer concentration at $Re = 73$. Left column: $tU_0/D = 50$, right column: $tU_0/D = 800$. From top to bottom, $\tau U_0/D = 18.25$, 36.5, 73, and 146.

transition region where they remain separated (Fig. 26). The initial transition region depends on the characteristics of the ramp. The shorter the time constant of the exponential function, the shorter the initial transition region. However, the flow behavior at long term is not significantly altered by the ramp characteristics.

The effect of the wall thickness at nozzle distances far from the wall can be observed in Fig. 27. A case of thick and thin wall is presented (thickness: 2 diameters and 0.1 diameters, respectively). The effect is rather moderate and we can observe slight modifications on the positions of the collapse of the curves, being closer to the nozzle exit for the case with a thick wall.

It is important to signal here that even though the flows considered are fundamentally non-linear, it is remarkable that the creeping flow solutions remain a good frame of reference for the analysis. The initial transition region lies clearly outside the region of validity of this solution. However as the

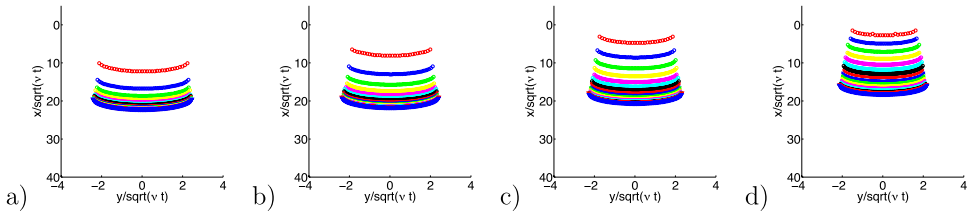

FIG. 26. Frontlines in terms of similarity variables considering different ramps. $Re = 73$, (a) $\tau U_0/D = 18.25$, (b) $\tau U_0/D = 36.5$, (c) $\tau U_0/D = 73$, and (d) $\tau U_0/D = 146$.

vortex structure travels downstream, it decreases its velocity, viscous effects become non-negligible and the self-similar behavior takes place. This indicates that the starting jet exhibits, as other flows, a rather robust self-similar behavior with a relative rapid loss of memory of the initial conditions of the flow. Thus, the flow in the symmetric regime can be considered a class of processes that is locally (as opposed to globally) self-similar.

B. Wall dominated regime

We can mention two effects associated with the wall presence that alter the dynamics of the vortex head observed in the symmetric regime. A first effect is related to an image vortex, and a second effect is related to the non-slip condition at the wall. Both effects also exist in the case of vortex ring interactions with a wall as described in the literature.[13] The first effect is a non-viscous interaction which initially produces a slight approach of the vortex head to the wall. We can consider, to illustrate this effect, a nonviscous model for the head, which consists in assuming that the vorticity distribution agrees with Hill's spherical vortex model.[40] This model is based on the hypothesis that the vorticity is confined to the interior of a sphere that moves with uniform velocity. Evaluation of the effect of the wall is immediate considering the image vorticity that annihilates the normal velocity at this boundary.[41] In Fig. 28, we show the results considering this kind of model. As we can see the decrease in pressure in the region existing between the sphere and wall attracts the head towards the surface.

To illustrate the second "viscous" effect, we consider results of the 3D numerical simulation (see Fig. 29).

The nonslip condition produces new secondary vorticity of opposite sense to that of the vortex head along the boundary. The mutual interaction of vorticity is stronger with the vortex segments of the head that are located closer to the wall than with those that are further away. As a result of this process, the spinning of the part of the head that moves at larger distances from the wall is altered less than the one at closer distances from it. This drives the lower structure to the upper mid-plane. The retardation of fluid at the vicinity of the wall is also accompanied by an increase in pressure that also pushes the vortex head upwards. As the torus of the vortex ring changes its shape, the different constitutive segments no longer have the same curvature radius. The induced velocity is no longer the same in the different vortex segments. The segments lying in the proximity of the horizontal mid-plane, which

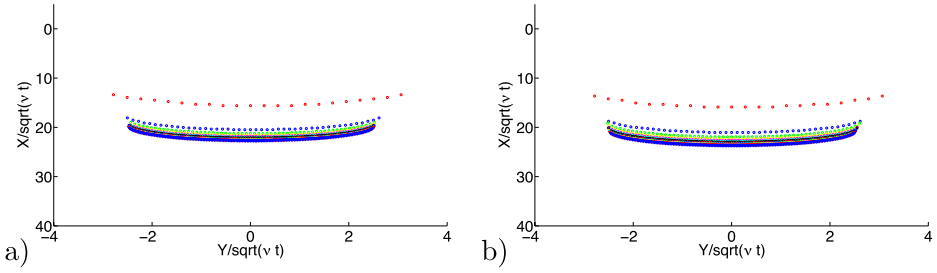

FIG. 27. Frontlines in terms of similarity variables considering different wall sizes of the nozzle, with a step ramp; (a) thick nozzle (wall thickness: 2 diameters); (b) thin nozzle (wall thickness: 0.1 diameters).

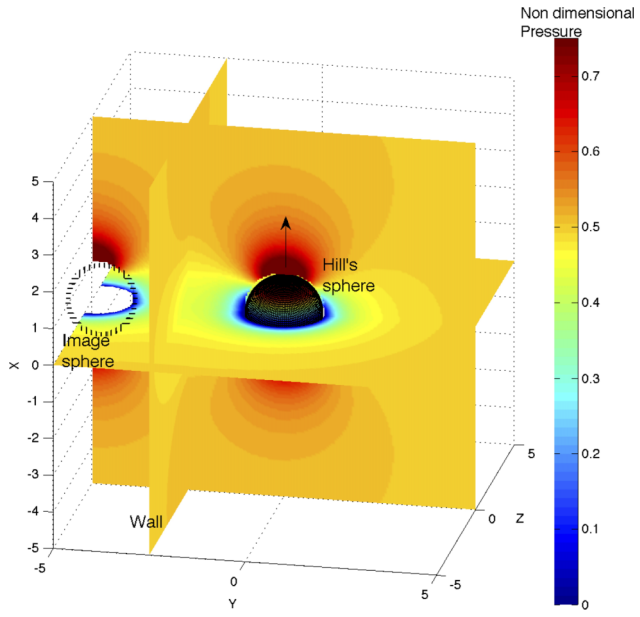

FIG. 28. Nondimensional pressure field for the Hill's sphere model of unit radius with a wall. Movement of the sphere is vertical and wall is placed vertically.

as a consequence of deformation have diminished their radius, tend to move faster in the horizontal direction than those of the upper segment. The process continues until only one vortex structure can be identified in the head, in which the upper structure cannot be distinguished from the lower one.

Concerning the incidence of wall thickness when the nozzle is disposed at close vicinity to the wall, we can indicate that the thick wall slightly retards the front position when compared to the thin wall simulation, much like the axisymmetric case. There is also a slightly higher approximation of the jet stem to the wall in the case of the thick wall, but the effect is not significant. Snapshots of the 3D

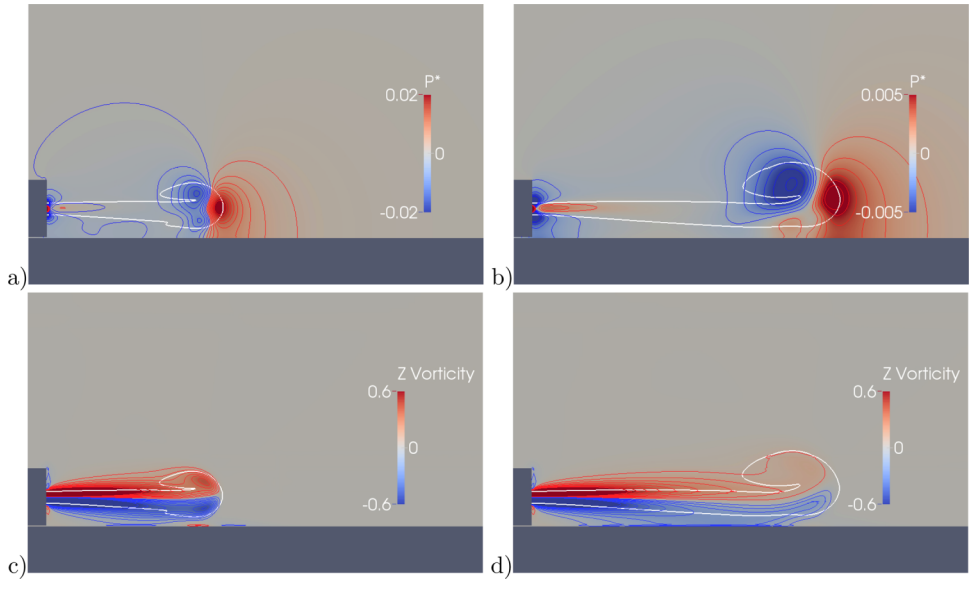

FIG. 29. 3D numerical simulations, $Re = 73$, $d = 0.26$ mm, and thick wall nozzle. At the top line: Pressure fields. At the bottom line: Z-vorticity fields. At left, the nozzle exit for nondimensional time $t \times U_0/D = 40$, and at right, a larger view for $t \times U_0/D = 110$. The white line is a tracer iso-contour.

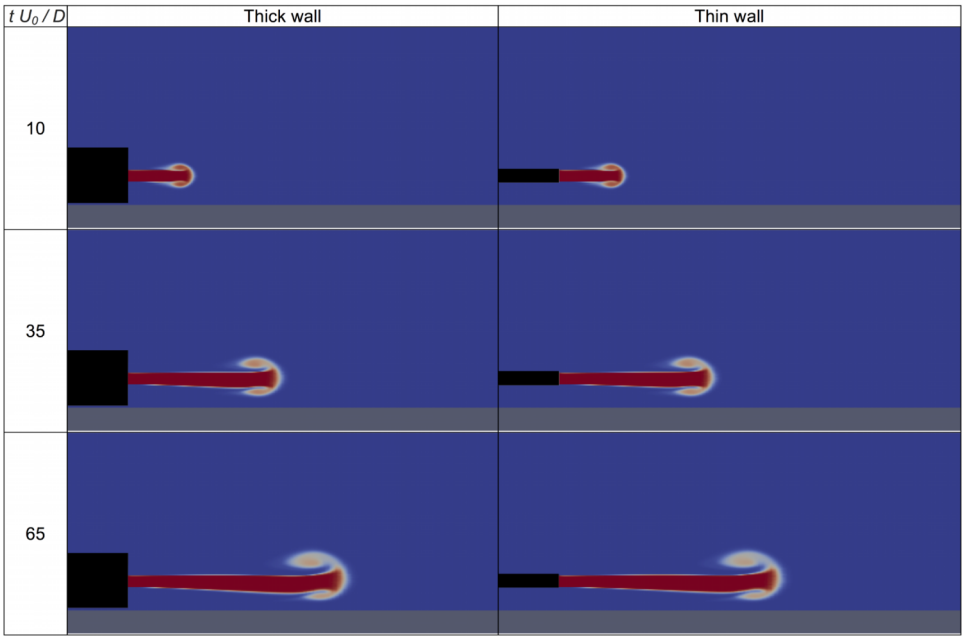

FIG. 30. 3D numerical simulations to illustrate effect of the wall thickness. Snapshots of tracer isocontours at three different nondimensional times: $tU/D = 10$, 35, and 65. $Re = 73$. $d/D = 2.6$. Left: Thick nozzle (wall thickness: 2 diameters). Right: Thin nozzle (wall thickness: 0.1 diameters).

numerical simulations at $Re = 73$ illustrate this and can be found in Fig. 30. Snapshots there appearing correspond to four different nondimensional times: $tU/D = 10$, 35, and 65 (which are equivalent to $t = 1.4$, 4.8, and 8.9 ms).

The evolution from a dipolar-like structure to a monopolar-like structure occurs also in transient wall jets.[42] Similarity has been found only for the steady wall jets. In the transient case described, however, as the vortex structures evolve in shape with large distortions, it is difficult to expect some kind of similarity during this transition. Once the flow adopts a monopolar configuration that travels in proximity to the wall, there exists some potential to find a self-similar behaviour. This vortex structure in the plane normal to the wall containing the jet axis is reminiscent of a planar junction vortex pattern. Such kind of flows take place in the regions close to the junction of an impulsively started plate. Similarity analysis for this kind of flow has been previously reported.[43] Early stages of these flows are viscous dominated, and at larger times, they become inertia dominated. In consequence, for this last stage, scaling is different than the one considered in Cantwell's study. In the case we study, the two-dimensionality of the flow that is present in the junction vortex flow is also absent, except on the plane of symmetry where this condition is fulfilled. It is on this plane that we focus our analysis.

1. Scaling laws

The main aspect that may break the dilation group invariance of the problem in this regime is related to the boundary condition imposed by the wall. In this problem, the invariance of the boundary condition under this transformation is no longer assured, and thus self-similarity is not expected in all regions of the flow.

Fig. 31 shows the frontlines in terms of the similarity variables $x/sqrt(\nu t)$ and $y/sqrt(\nu t)$ experimentally obtained. As we can see, the frontlines are tilted as a consequence of the wall presence. After a initial interval in which the curves in nondimensional variables do not superpose, a good collapse of the curves is observed. The first interval depends on the nozzle-wall distance. The collapse of the curves attained indicates that the self-similar behavior occurs for the larger times. At this stage, the flow adopts at the symmetry plane a monopolar-like configuration, reminiscent of the junction vortex structure.

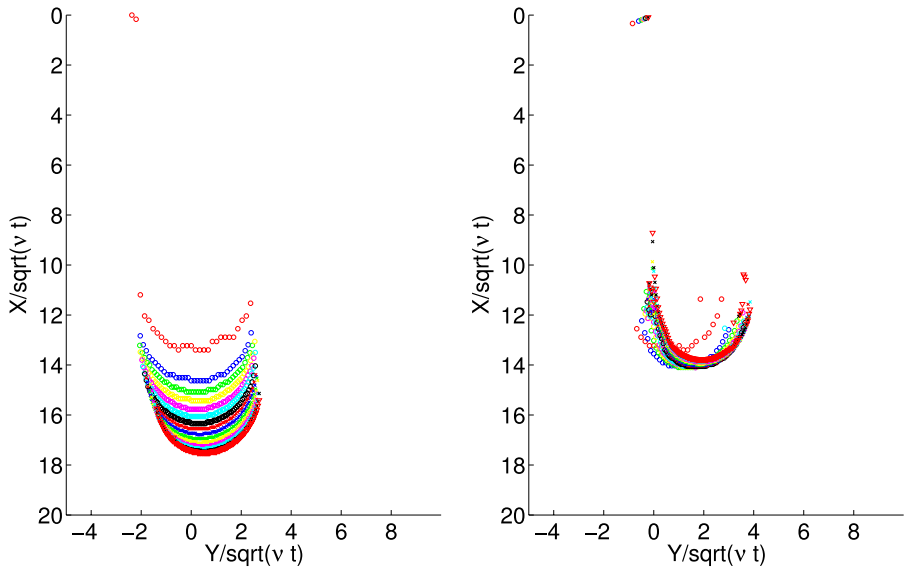

FIG. 31. Frontlines in terms of similarity variables considering time steps of 33.3 ms starting at 33.3 ms (symbols agree with those of Figure 15); (a) $Re = 73$; $d = 1.6$ mm; (b) $Re = 73$; $d = 0.26$ mm.

Inspired in Allen and Naitoh's[43] findings, we can propose for this stage a fit of the horizontal front position with a power-law of the type

$$\left(\frac{U_0^2 t}{\nu}\right)^m = k\left((X_F - X_0)\frac{U_0}{\nu}\right)^n = k\left(Re_F \frac{U_0}{U_F}\right)^n. \tag{12}$$

In this expression, we observe a new scaling for the horizontal front position $X_F{}^* = \frac{X_F U_0}{\nu}$ and for the time $t^* = \left(\frac{U_0{}^2 t}{\nu}\right)$. Allen and Naitoh[43] found for the movement of the junction vortex that the values of both power coefficients (m and n) were close to unity. This kind of scaling has been used however by these authors to describe the inertia dominated regime of the junction vortex flow. When $m = 1/2$ and $n = 1$, inertia and viscous scalings are coincident. We represent in Fig. 32 X_F^* against $sqrt(t^*)$. The graphs show that, for early times, the constant k is higher than when the wall effect is present at larger times. At the last stages the value of k seems to remain constant in all cases. For a given Re, the function k for large times has a poor dependency on the value of the nozzle-wall distance d. Moreover, for a given nozzle-wall distance, the function k for large times adopts similar values. Initiation of the viscous-wall dominated regime can be associated with the instant in which the value of k attains a constant value along time. This time is larger for the larger exit jet velocities and for the larger nozzle-wall distances.

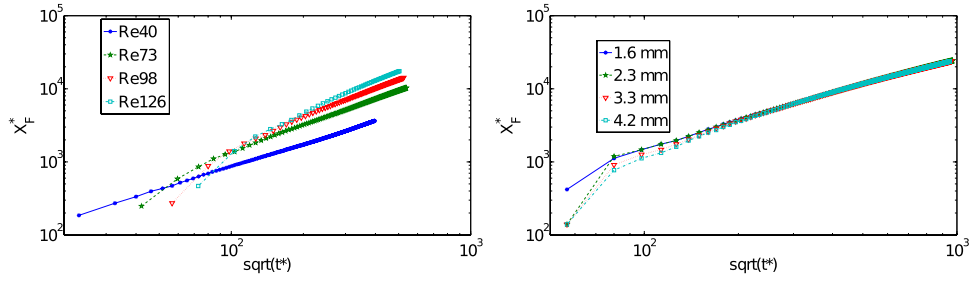

FIG. 32. Nondimensional horizontal front position as a function of the square root of the nondimensional time. Left figure: Starting jet at different Reynolds numbers (40, 73, 98, and 126) and 5.4 mm nozzle-wall distance. Right figure: Starting jet with Reynolds number 98 at different nozzle-wall distances (1.6, 2.3, 3.2, 4.2 mm).

In short we observed that at the plane of symmetry, the flow in the wall regime can be considered a class of processes that is locally (as opposed to globally) self-similar. This process is preceded by an initial transition region where the flow does not present this characteristic. This stage, where the dipolar structures are altered by the presence of the wall, is not of a self-similar class. As the vortex head structure travels downstream and adopts a monopolar-like structure, the self-similar behavior takes place. This indicates that the starting jet in the wall type regime, and in the symmetric regime as well, develops a self-similar behavior that has a relative rapid loss of memory of the preceding condition of the flow. Scaling for both regimes are those that correspond to viscous dominated flows.

V. CONCLUSIONS

We consider a starting laminar immersed jet issuing from a long micropipette with a wall placed tangentially at close proximity to the exit orifice. The flow can be characterized by a vortex head followed by a stem jet. Our study distinguishes from many previous studies of the free laminar starting jet since the effects of instabilities in the flow we study, and especially those of the stem jet, are negligible. We could identify two regimes. A symmetric regime in which the behavior is not influenced by the wall, and a second regime in which the wall introduces modifications to the flow patterns. The size of the vortex head increases with time, and once it attains a radius close to half of the nozzle-wall distance, it loses the axial symmetry. The time required for the transition into the second regime appears to be proportional to $Re^{-2.5}$. We analyzed the movements of three points of the vortex head: the *front*, *top*, and *bottom* points. The horizontal velocity of the last two points is lower than that of the *front* point. In the symmetric regime, we found a similar behavior of the front velocity of the starting jet with the one observed in steady jets: namely, a linear decay of the velocity with the inverse of the distance to the nozzle exit and a correction of this axial distance with a virtual jet origin. A good fit of Landau's constant can be obtained with $Re^{2.5}$, which is larger than the values found by Andrade and Tsien.[35] The dependence of Landau's constant with respect to Reynolds number differs comparing starting jets with steady jets. In the symmetric regime, the *top* and *bottom* points move describing a constant angle that decays as Reynolds number increases. The axis of the jet stem remains rectilinear during this regime and the jet opens with a small angle.

In the wall dominated regime, the spiralled vortex of the head does not form a torus any longer. The structure is deformed and the lower segment moves away from the wall. The *front* point velocity exhibits a vertical component in this regime and the head tends to increase its distance to the wall. The vertical velocity component monotonically increases with Reynolds number and decreases as the distance to the wall increases.

Compared to the symmetric regime, the horizontal velocity of the *front* is slightly retarded, and the *top* and *bottom* points do not separate any longer with a constant angle. In the first stages of the wall dominated regime, the *front* position varies linearly with the square root of the time and it is still possible to fit the horizontal *front* positions with similar laws than the one observed for the symmetric regime, but Landau's constant and the virtual origin have to be slightly modified.

The vertical mid-plane of the flow is still a symmetry plane. In this plane, at very long times, the head structure is reminiscent of the junction vortex. Due to the movement of the head in the wall dominated regime, the axis of the jet stem does not remain rectilinear and bends first approaching the wall and then separating from it.

We have analysed the self-similar behavior of the flow in the symmetric and wall dominated regimes. We restricted this analysis to a single plane and concentrated our analysis mainly on the frontline dynamics as we can identify this line easily in the portrait of particle paths. We observed that in the symmetric and wall dominated regimes, it is possible to find a class of processes that is locally (as opposed to globally) self-similar. This kind of process is preceded by an initial transition region where the flow does not present this characteristics. In the symmetric regime, this transition phase depends, among other parameters, on the process of injection of fluid. In the wall dominated regime, this first stage is associated with a process in which the dipolar structures are altered by the presence of the wall. As the vortex head structure travels downstream and adopts a monopolar like structure, self-similar behavior takes place. These kind of results indicate that the starting jet in the wall type regime, and in the symmetric regime as well, develops a self-similar behavior that has a

relative rapid loss of memory of the preceding condition of the flow. Scaling for both regimes are those that correspond to viscous dominated flows.

ACKNOWLEDGMENTS

This work has been supported in part by the Argentinian ANPCyT through the Project No. PRH-PICT 2008-250.

[1] J. M. Cabaleiro and J.-L. Aider, "Axis-switching of a micro-jet," Phys. Fluids **26**, 031702 (2014).
[2] M. J. Rodriguez, I. Iscla, and L. Szczupak, "Modulation of mechanosensory responses by motoneurons that regulate skin surface topology in the leech," J. Neurophisiol. **91**, 2366–2375 (2004).
[3] J. O. Dabiri, "Optimal vortex formation as a unifying principle in biological propulsion," Annu. Rev. Fluid Mech. **41**, 17–33 (2009).
[4] B. J. Cantwell, "Viscous starting jets," J. Fluid Mech. **173**, 159–189 (1986).
[5] S. Abramovich and A. Solan, "The initial development of a submerged laminar round jet," J. Fluid Mech. **59**, 791–801 (1973).
[6] J. S. Turner, "A comparison between buoyant vortex rings and vortex pairs," J. Fluid Mech. **7**, 419–432 (1960).
[7] L. Gao and S. C. M. Yu, "A model for the pinch-off process of the leading vortex ring in a starting jet," J. Fluid Mech. **656**, 205–222 (2010).
[8] M. Shusser and M. Gharib, "A model for vortex ring formation in a starting buoyant plume," J. Fluid Mech. **416**, 173–185 (2000).
[9] L. Gao, S. C. M. Yu, J. J. Ai, and A. W. K. Law, "Circulation and energy of the leading vortex ring in a gravity-driven starting jet," Phys. Fluids **20**, 093604 (2008).
[10] H. Helmholtz, "On the integrals of the hydrodynamical equations, which express vortex-motion," Philos. Mag. Ser. 4 **33**(226), 485–512 (1867).
[11] O. Reynolds, "On the resistance encountered by vortex rings, and the relation between the vortex rings and streamlines of a disk," Nature **14**, 477–579 (1876).
[12] K. Shariff and A. Leonard, "Vortex rings," Annu. Rev. Fluid Mech. **24**, 235–279 (1992).
[13] T. T. Lim and T. B. Nickels, "Vortex rings," in *Fluid Vortices*, edited by S. I. Green (Kluwer Academic Publishers, 1995).
[14] W. Zhao, H. S. Frankel, and L. G. Mongeau, "Effects of trailing jet instability on vortex ring formation," Phys. Fluids **12**, 589–596 (2000).
[15] P. O. Witze, "The impulsively started incompressible turbulent jet," Technical Report SAND80-8617, Sandia National Labs., 1980.
[16] P. Ouellette and P. G. Hill, "Turbulent transient gas injections," J. Fluids Eng. **122**, 743–752 (1999).
[17] S. C. Crow and F. H. Champagne, "Orderly structure in jet turbulence," J. Fluid Mech. **48**, 547–591 (1971).
[18] I. Danaila, J. Dusek, and F. Anselmet, "Coherent structures in a round, spatially evolving, unforced, homogeneous jet at low reynolds numbers," Phys. Fluids **9**, 3323–3342 (1997).
[19] P. J. Morris, "The spatial viscous instability of axisymmetric jets," J. Fluid Mech. **77**, 511–529 (1976).
[20] T. C. Corke, F. Shakib, and H. M. Nagib, "Mode selection and resonant phase locking in unstable axisymmetric jets," J. Fluid Mech. **223**, 253–311 (1991).
[21] P. O'Neill, J. Soria, and D. Honnery, "The stability of low Reynolds number round jets," Exp. Fluids **36**, 473–483 (2004).
[22] A. J. Reynolds, "Observations of a liquid-into-liquid jet," J. Fluid Mech. **14**, 552–556 (1962).
[23] J. C. Mollendorf and B. Gebhart, "An experimental and numerical study of the viscous stability of a round laminar vertical jet with and without thermal buoyancy for symmetric and asymmetric disturbances," J. Fluid Mech. **61**, 367–399 (1973).
[24] C. Gau, C. H. Shen, and Z. B. Wang, "Peculiar phenomenon of micro-free-jet flow," Phys. Fluids **21**, 092001 (2009).
[25] V. M. Aniskin, D. A. Bountin, A. A. Maslov, S. G. Mironov, and I. S. Tsyryulnikov, "Stability of a subsonic gas microjet," Tech. Phys. **57**, 174–180 (2012).
[26] D. Rockwell, "Vortex-body interactions," Annu. Rev. Fluid Mech. **30**, 199–229 (1998).
[27] T. L. Doligalski, C. R. Smith, and J. D. A. Walker, "Vortex interactions with walls," Annu. Rev. Fluid Mech. **26**, 573–616 (1994).
[28] T. T. Lim, "An experimental study of a vortex ring interacting with an inclined wall," Exp. Fluids **7**, 453–463 (1989).
[29] V. O'Loughlin and D. Bohl, "Convection of a vortex ring parallel to a plane wall," in *Proceedings 63rd Annual Meeting of the APS Division of Fluid Dynamics* (APS, 2010).
[30] G. Singh, T. Sundararajan, and K. A. Bhaskaran, "Mixing and entrainment characteristics of circular and noncircular confined jets," J. Fluids Eng. **125**, 835–842 (2003).
[31] D. Koller-Milojevie and W. Schneider, "Free and confined jets at low Reynolds numbers," Fluid Dyn. Res. **12**, 307–322 (1993).
[32] L. Prandtl, "Über die entstehung von wirbeln in der idealen flüssigkeit, mit anwendung auf die tragflügeltheorie und andere aufgaben," in *Vorträge aus dem Gebiete der Hydro- und Aerodynamik (Innsbruck 1922)*, edited by T. v. Kármán and T. Levi-Civita (Springer, Berlin Heidelberg, 1924), pp. 18–33.
[33] M. Hettel, F. Wetzel, P. Habisreuther, and H. Bockhorn, "Numerical verification of the similarity laws for the formation of laminar vortex rings," J. Fluid Mech. **590**, 35–60 (2007).
[34] L. D. Landau and E. M. Lifshitz, *A Course of Theoretical Physics* (Pergamon Press, 1959), Vol. 6, p. 107.
[35] E. N. da C Andrade and L. C. Tsien, "The velocity distribution in a liquid-into-liquid jet," Proc. Phys. Soc. **49**, 381 (1937).
[36] D. Sciamarella, F. Silva, and G. Artana, "Similarity analysis of a glottal like jet," Exp. Fluids **53**, 765–776 (2012).
[37] F. Archambeau, N. Méchitoua, and M. Sakiz, "Code saturne: A finite volume code for the computation of turbulent incompressible flows," Int. J. Finite Vol. **1** (2004), available at http://www.latp.univ-mrs.fr/IJFV/spip.php?article3.

[38] V. Kurdyumov, "Far-field description of the flow produced by a source of both momentum and mass," J. Fluid Mech. **532**, 191–198 (2005).
[39] C. Sozou, "Development of the flow field of a point force in an infinite fluid," J. Fluid Mech. **91**, 541–556 (1979).
[40] M. Hill, "On a spherical vortex," Philos. Trans. R. Soc., A. **185**, 213–245 (1894).
[41] P. Saffman, *Vortex Dynamics*, Cambridge Monographs on Mechanics (Cambridge University Press, 1992).
[42] B. Conlon and S. Lichter, "Dipole formation in the transient wall jet," Phys. Fluids **7**, 999–1014 (1995).
[43] J. J. Allen and T. Naitoh, "Scaling and instability of a junction vortex," J. Fluid Mech. **574**, 1–23 (2007).